Environmental Science and Engineering

Sijing Wang
Runqiu Huang
Rafig Azzam
Vassilis P. Marinos *Editors*

Engineering Geology for a Habitable Earth: IAEG XIV Congress 2023 Proceedings, Chengdu, China

Volume 3: Active Tectonics, Geomorphology, Climate and Geoenvironmental Engineering Geology

Springer

Environmental Science and Engineering

The ultimate goal of this series is to contribute to the protection of our environment, which calls for both profound research and the ongoing development of solutions and measurements by experts in the field. Accordingly, the series promotes not only a deeper understanding of environmental processes and the evaluation of management strategies, but also design and technology aimed at improving environmental quality. Books focusing on the former are published in the subseries Environmental Science, those focusing on the latter in the subseries Environmental Engineering.

Sijing Wang · Runqiu Huang · Rafig Azzam ·
Vassilis P. Marinos
Editors

Engineering Geology for a Habitable Earth: IAEG XIV Congress 2023 Proceedings, Chengdu, China

Volume 3: Active Tectonics, Geomorphology, Climate and Geoenvironmental Engineering Geology

Springer

Editors
Sijing Wang
Department of Hydraulic Engineering
Tsinghua University
Beijing, China

Rafig Azzam
Department of Engineering Geology
and Hydrogeology
RWTH Aachen University
Aachen, Germany

Runqiu Huang
Chengdu University of Technology
Chengdu, Sichuan, China

Vassilis P. Marinos
School of Civil Engineering
National Technical University of Athens
Zografou, Greece

ISSN 1863-5520 ISSN 1863-5539 (electronic)
Environmental Science and Engineering
ISBN 978-981-99-9064-1 ISBN 978-981-99-9065-8 (eBook)
https://doi.org/10.1007/978-981-99-9065-8

Academic Committee

Academic Committee Chairs

Sijing Wang
Runqiu Huang

Academic Committee Members

Anthony Bowden
Bin Shi
Bo An-Jang
Carlos Delgado
Charles W. W. Ng
Chungsik Yoo
Defang Kong
Dingcheng Huang
Faquan Wu
Fawu Wang
Helen Reeves
Hengxing Lan
Hsein Juang
Huiming Tang
Janusz Wasowski
Jean Hutchinson
Jean-Alain Fleurisson
Jian Yang
Jianbing Peng
Jianmin Zhang
Jianxin Hua

Jinxiu Yan
John Ludden
Julien Cohen-Waeber
Kyoji Sassa
Lansheng Wang
Manchao He
Martin Culshaw
Moshood Niyi Tijani
Nicola Casagli
Niek Rengers
Peng Cui
Qing Wang
Rafig Azzam
Ranjan Kumar Dahal
Resat Ulusay
Ricardo Oliveira
Roger Frank
Scott F. Burns
Shitian Wang
Shutao Yang
Vassilis P. Marinos
Victor Manuel Hernandez Madrigal
Wei Wu
Wei Zhang
Xiao Li
Xiating Feng
Yong-Seok Seo
Yueping Yin
Yusheng Gao
Zelian Chen
Zuyu Chen

Organizing Committee Chairs

Qiang Xu
Qiangbing Huang
Shengwen Qi
Xiangjun Pei
Xiaoqing Chen
Yuyong Jiao
Xuanmei Fan

Organizing Committee Members

Chaojun Ouyang
Chaosheng Tang
Jianjun Zhao
Liangqing Wang
Ning Liang
Wen Zhang
Yuhuan Song

Preface

The XIV Congress of the International Association for Engineering Geology and the Environment (XIV IAEG Congress 2023) was successfully held in Chengdu, China, from September 21 to 27, 2023. Focusing on the main theme "Engineering Geology for a Habitable Earth", researchers and practitioners worldwide from academia, industry, and government have joined us in this prestigious event. Based on the topics discussed at the congress, the proceedings are organized into six volumes as follows:

- Volume 1: Engineering Geomechanics of Rock and Soil Masses
- Volume 2: Geohazard Mechanisms, Risk Assessment and Control, Monitoring and Early Warning
- Volume 3: Active Tectonics, Geomorphology, Climate and Geoenvironmental Engineering Geology
- Volume 4: Technological Innovation and Applied for Engineering Geology
- Volume 5: Megacity Development and Preservation of Cultural Heritage Engineering Geology
- Volume 6: Marine and Deep Earth Engineering Geology

Meanwhile, on behalf of the organizing committee, we would also like to express our deepest appreciation to the technical program committee members, reviewers, session chairs, and volunteers for their strong support for congress.

Last but not least, our gratitude also goes to the editors and press for their great support to the congress.

IAEG XIV Congress 2023 Organizing Committee

Beijing, China — Sijing Wang
Sichuan, China — Runqiu Huang
Aachen, Germany — Rafig Azzam
Zografou, Greece — Vassilis P. Marinos
September 2023

Contents

Chapter 1
Study on the Deformation Zone of Tianzhuang Fault in Taiyuan, China

Han Xiaofei, Dong Bin, Shi Shuangshuang, and Xue Xiaodong

Abstract The burial depth in modern urban lifeline engineering, subway construction, and the foundations of super high-rise buildings can reach depths of up to 30 m or even deeper. Therefore, when dealing with buried faults at depths less than 60 m, it becomes essential to assess their seismic activity and study their paleo-earthquake recurrence cycles. This research holds great significance for enhancing engineering earthquake resistance and mitigating fault-related risks. The Tianzhuang fault is a concealed fault of considerable importance, exhibiting clear activity during the late Pleistocene in the Taiyuan Basin, Shanxi Province, China. This study begins by analyzing the regional geological tectonic background and subsequently delves into the tectonic processes associated with the Yanshan and Xishan movements within the Tianzhuang fault. The temporal and spatial activity characteristics of multi-stage faults are examined through the processing and interpretation of shallow seismic profiles of the Tianzhuang fault. Further insights are gained through ground deformation surveys and an analysis of borehole joint sections, which allow us to present details of the recently displaced strata in the primary section. These efforts contribute to the verification of a fault gas anomaly zone within the concealed fault and the confirmation of the extent of the deformation zone within the Tianzhuang fault since the late Pleistocene. Ultimately, this research enables the dynamic visualization of the main fault's shifting location and the formation and expansion of the fault zone within the Jiaocheng fault zone.

Keywords Tectonic history · Shallow earthquake · Borehole joint profile · Fault gas · Deformation zone

H. Xiaofei (✉) · D. Bin · S. Shuangshuang · X. Xiaodong
Seismological Bureau of Shanxi Province, Taiyuan, China
e-mail: 38094048@qq.com

S. Wang et al. (eds.), *Engineering Geology for a Habitable Earth: IAEG XIV Congress 2023 Proceedings, Chengdu, China*, Environmental Science and Engineering,
https://doi.org/10.1007/978-981-99-9065-8_1

1.1 Introduction

The caprock of the North China block primarily comprises Mesoproterozoic shallow metamorphic rocks, a Cambrian-Ordovician deep-sea facies sedimentary rock series, a Carboniferous-Permian interplay of marine and terrestrial rock series, as well as volcanic facies and Mesozoic and Cenozoic terrigenous clastic facies sedimentary rock series. Notably, there is generally an absence of Upper Ordovician, Silurian, Devonian, and Cenozoic-Paleocene layers, with the basement consisting of Archean and Paleoproterozoic deep metamorphic rock series (Zhu et al. 2019).

According to the research results of structural geology and chronology, the age of the A-episode of the Yanshan movement was about 165 Ma. The most significant sign is the angular unconformity event widely developed in the North China Craton in the late Jurassic. The corresponding tectonic environment is in a compressive state, with a duration of about 5 Ma, resulting in the translation of the a-episode of the Yanshan movement and the Tanlu fault on the surface of the active continental margin; The crustal shortening, folding and stratigraphic angular unconformity events widely developed in the North China Craton around 138Ma marked the occurrence of the B-episode of the Yanshan movement. At this time, Eastern China was represented by a compression event, and the Tan Lu fault zone shifted leftward again, the basin reversed and the short-term regional uplift; The geodynamic mechanism causing the B-episode of Yanshan movement is that the subduction angle of the Western Pacific plate gradually decreases (Xu et al. 2013).

The nearly north–south trending high angle normal faults developed in front of Taihang mountains and along the southern segment of Tanlu fault zone in North China were formed in 75 ~ 65 Ma. These faults are also the products of marginal faults or initial rifts in North China Basin. With these deformations, a large number of volcanic activities developed along the southern segment of the Tan Lu fault zone. The formation of the Cenozoic North China basin is based on this (Wang, et al., 2018).

Shortly after the initial India-Asia collision (10–20 Ma), the upper crust of the Himalayas was thickened to the lower crust of > 35 km and produced anatexis. This earliest crustal thickening event was completely coupled with the era of residual epicontinental regression events recorded in foreland sub-basins such as Subathu in northwest India and Tansen in Nepal, which was the inducement of the initial uplift of the Himalayas. In other words, the Himalayas initially rose above sea level by crustal thickening at about 44–38 Ma (Huang 2021).

The research results of thermochronology and fission track in recent years show that the initial plateau experienced the initial uplift of 24–17 Ma and the denudation, planarization and pene planarization of 17–3.6 Ma during the Neogene, forming the main plantation plane of the plateau; At 3.6 Ma, the main planation surface of the plateau disintegrated, the terrain around the plateau changed sharply, the conglomerate of Xiyu formation with a thickness of 2000-3000 m in the southern margin of the Himalayas, and the conglomerate of Dayi formation (Q_1) of lower Pleistocene in front of Longmen Mountain showed a large and rapid uplift in the hinterland of the

plateau from late Pliocene (about 4–3.6 Ma) to late Early Pleistocene (0.9–0.8 Ma) (corresponding to the third episode of Himalayan), Today's Qinghai Tibet Plateau and its peripheral plateaus finally formed (Ge, et al., 2010).

The sedimentary strata also prove that the Himalayan orogeny at the end of the Paleogene (24 Ma ±) caused major turning changes in China and even the Asian continent, and a series of fault basins in eastern China entered the overall depression stage (Huang, et al. 2012).

To sum up, according to the direction and sequence of subduction and retreat of the Pacific plate, the tension pattern of the Jiaocheng fault in the Fenwei Rift was formed 75 ~ 65 Ma earlier. The first retreat of the Pacific plate started at 130 Ma in the Early Cretaceous and began to shape the embryonic form of the Taiyuan basin.

1.2 Understanding of Tianzhuang Fault

The regional stress field changed in the Cenozoic, and the thrust faults formed in the Mesozoic were reversed by north–south dextral shear. Firstly, the thrust fault on the Zhongtiaoshan Wanrong anticline was faulted, and Oligocene and Miocene sediments were deposited, which are Yuncheng sag and Houma sag. Subsequently, in Pliocene, the Jiaocheng reverse fault on the northwest wing of Taiyueshan anticline, the Huoshan-Luoyunshan fault on the West Wing of Huoshan Matoushan anticline and its longitudinal and transverse fractures, as well as the western end of the conjugate fracture on Taiyueshan anticline also took place, gradually forming Taiyuan fault basin and Linfen fault basin (Xie et al. 1996).

The thrust section of Jiaocheng fault formed by Yanshan movement basically tilts southeast. Its dip angle ranges from high angle to low angle. All the old rock series on the east side are pushed over the new rock series to the West. In the Himalayan period or Neogene Period, the block on the original east side of the upper wall fell down along the east foot of the Xishan mountains or roughly parallel to the original thrust fault line; However, the block on the lower wall of the original west side rises relatively, so the neotectonic movement begins. The east side receives new sediments and alluvium to become a plain, and the west side rises to form a platform. This differentiation movement is still mainly carried out intermittently, which is the main factor that makes the east foot of the West Mountain steep (Pan 1957).

Jiaocheng fault generally strikes NE, starting from Fenyang, Wenshui, Jiaocheng and Qingxu in the south to the west of Yuci (from Qingxu to the west of Yuci, also known as Tianzhuang fault). One branch cuts straight to the north, the fault line extends wavily, the section tends to SE, the fault dip is relatively steep, the footwall rises and the hanging wall falls, which is a tensile growth fault. From the seismic reflection profile and drilling results, it is found that the Taiyuan Basin receives the upper Neocene unified lower Pleistocene sedimentation. The sediment tilts slowly from east to west, and the thickness increases gradually. The thickness is the largest near the Jiaocheng fault, forming the sedimentary center. The deposition is wedge-shaped on the profile, indicating that the basin is controlled by the Jiaocheng fault. In

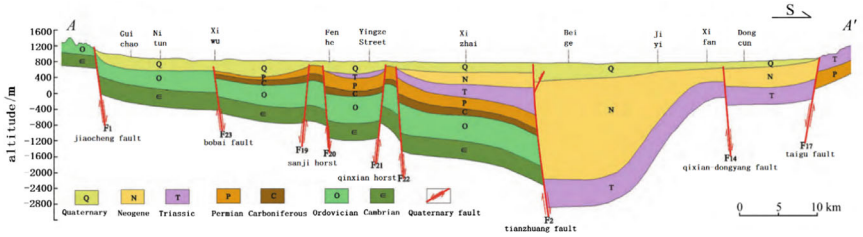

Fig. 1.1 SN geological section of Taiyuan Basin (Quoted from Zhang et al. 2020)

the hanging wall of the fault, there are nearly parallel small faults with low sequence and same direction (Yang et al. 1999; Zhang et al. 1996; Zhang et al. 2020; Han et al. 2017).

According to the velocity structure and seismic location, it is also proved that the Jiaocheng fault, as the main fault controlling the western edge of Taiyuan Basin, is a typical plow-type fault with a steep upper attitude and slow shovel lower attitude. Most of the earthquakes occurred near the fault (Wang, et al. 2014) (Fig. 1.1).

1.3 Location Change of Main Section of Tianzhuang Fault and Determination of Deformation Zone

1.3.1 Shallow Seismic Exploration Reveals

In September 2012, the Shanxi Institute of seismic engineering survey entrusted the Geophysical Exploration Center of China Seismological Bureau to carry out shallow seismic exploration of Tianzhuang fault. The wjb-xbg survey line starts from the highway intersection under construction in the north of Wenjiabao village in the north, passes through Songhuan village and Liujian village in the south, passes through ErGuang expressway, and ends in the field in the north of Xiaobeige village. See Fig. 1.2 for the location of the measuring line and section position.

It can be seen from Fig. 1.3 that the time profile of this survey line has a high signal-to-noise ratio, and a clear reflected wave group can still be seen at 1750ms of two-way travel time. There are abundant reflection wave groups in the section, which explains 11 strong reflection wave groups from top to bottom, and there are also abundant weak reflection wave groups between each wave group, which can be tracked continuously. The reflection interface characteristics revealed by each strong reflection wave group generally have the buried depth shape of deep in the South and shallow in the north. In the south of the section, there are abundant reflection wave groups, and each interface is distributed in nearly horizontal layers. The T_{Q+N} interface at the bottom continues to rise northward, and the T_{10} and T_{09} interfaces pinch out successively with the rise of T_{Q+N} interface. In the middle of the section,

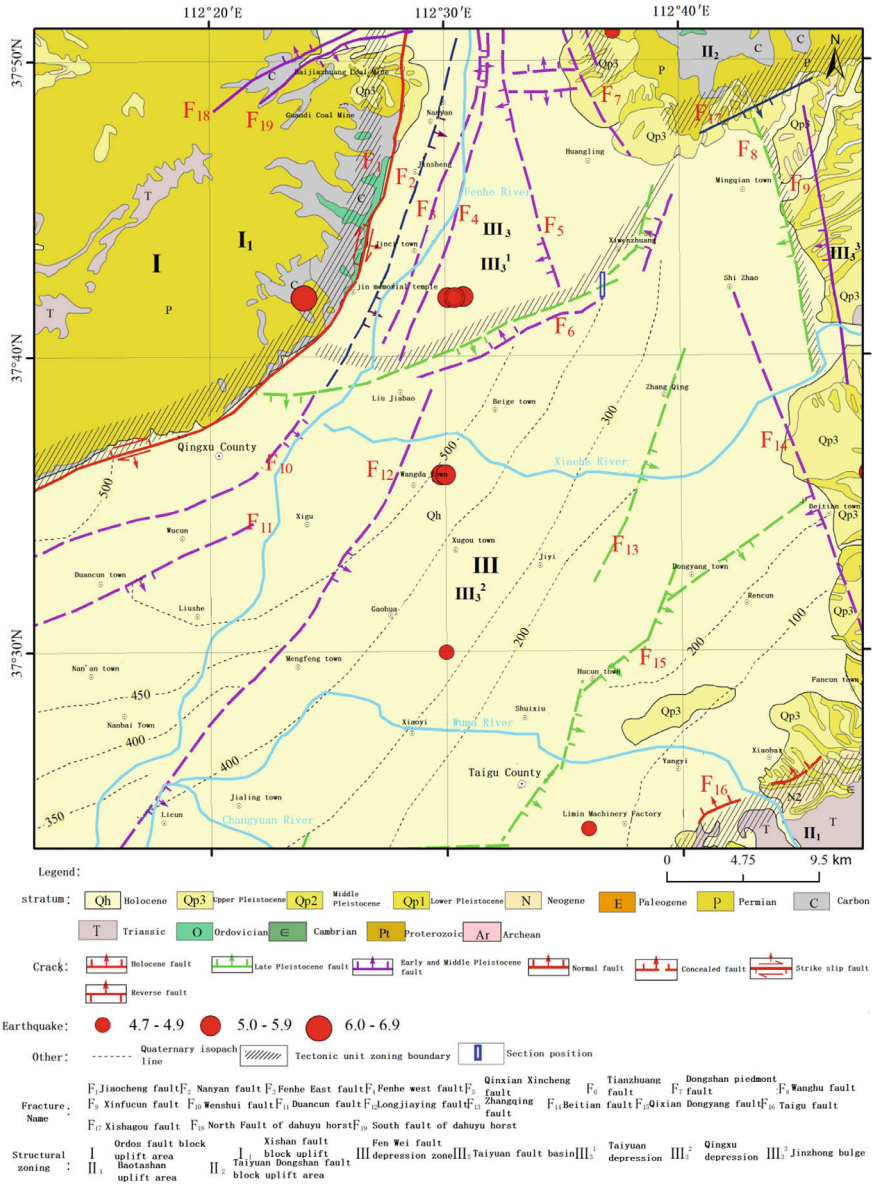

Fig. 1.2 Location of survey line and section and Seismotectonic background

the T_{Q+N} interface basically tends to be horizontal layered. On both sides of section stake No.790 m, there is obvious depth difference at T_{Q+N} interface, and the drop difference is about 700m; To the north of 790 m, T_{Q+N} interface is distributed in clear horizontal layers, and the interface is continuous. Combined with the characteristics of other shallow interfaces, it is considered that there is a phase of $F_{1\text{-}Qp3}$ and $F_{2\text{-}Qh}$ normal fault activity with an apparent dip to the south at section stake 790 m in the north section of the section. Combined with the tectonic activity history of the basin, it corresponds to the significant fault depression activity from the early late Pleistocene to now. Due to the difference in the identification of fault surface position caused by section interpretation, the distance between the two sections is about 300 m, In the Middle Pleistocene before the normal fault activity, thrust was the main activity, the basin uplifted and the denudation surface increased. The thrust activity in the Middle Pleistocene and the fault depression activity since the late Pleistocene formed a rolling anticline between section stake 640–940 m; At 1500 m of the section stake, there is also a period of strong fault subsidence activity, which corresponds to the third episode of Himalayan movement from Late Neogene to late Early Pleistocene of $F_{3\text{-}N}$ and $F_{4\text{-}Qp1}$. The fault subsidence amplitude is estimated to be 1900 m. This area also experienced compressive tectonic activity from middle Neogene to Late Neogene, resulting in the uplift of bedrock near the section; At 2400 m of the section stake, there are two sections formed by the fault subsidence activities of faults $F_{6\text{-}N}$ and $F_{5\text{-}N}$ in the early and middle Neogene. Because the bottom boundary of the hanging wall cannot be seen, it is impossible to estimate the fault subsidence amplitude. MLYL survey line is to further find out the structural characteristics of Tianzhuang fault at the bend.

From the section features (Fig. 1.4), the fault features are obvious, marked as $F_{2\text{-}Qh}$ and $F_{1\text{-}Qp3}$. There are regular faults at all interfaces interpreted in the section. The two-way travel time of 1000 ms can be recognized for the abundant reflection wave group in the south of $F_{1\text{-}Qp3}$, and only 360 ms TN interface can be recognized in the north of $F_{1\text{-}Qp3}$. The sedimentary characteristics of the strata on both sides of the breakpoint are obviously different, which is a normal fault inclined to the south. The upper breakpoint is located at a stake 690 m, the buried depth of the distinguishable upper breakpoint is about 50 ~ 55 m, and the vertical fault distance is about 3 ~ 4 m. Combined with the tectonic activity history of the basin, it corresponds to the significant fault depression activity from the early Late Pleistocene to now. Due to different activity periods, rolling anticlines are also formed between the two sections. This feature is very similar to the fault in this period in Fig. 1.1, and has also become the identification mark for the fault zone to track the fault in the same period in the basin. The distance between the breakpoints on the two sections is about 400m.

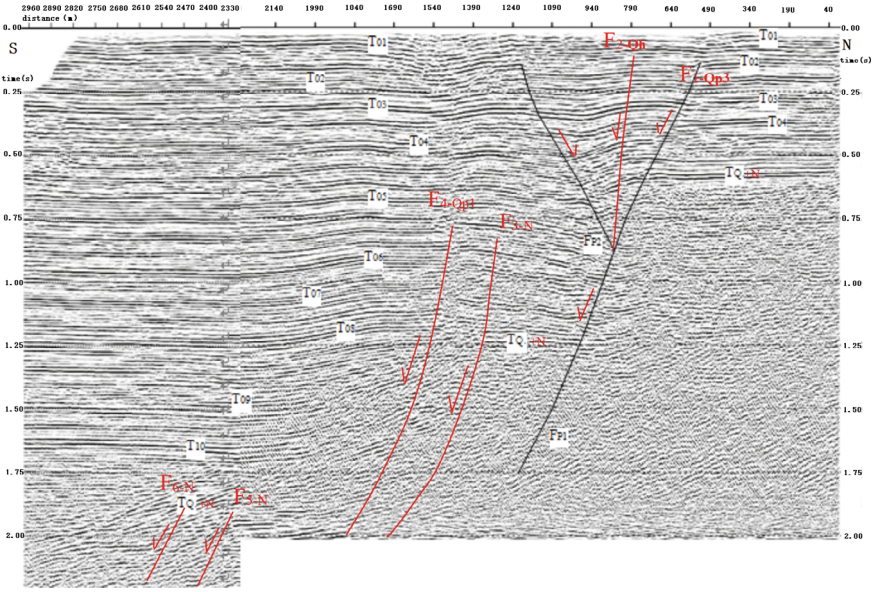

Fig. 1.3 Shallow seismic reflection time profile of Tianzhuang fault wjb-xbg survey line

1.3.2 Verification of Fault Gas on the Latest Active Main Section

According to the latest research results (Han x. et al. 2017), the most active part of Tianzhuang fault can be divided into the main front section $F2_{\text{-Qh}}$ and the main rear section $F1_{\text{-Qp3}}$, with a spacing of about 400 m. The deep part is the same main section, and the main front section $F2_{\text{-Qh}}$ and the main rear section $F1_{\text{-Qp3}}$ form an obvious stratigraphic arch area rolling anticline. See Figs. 1.5, 1.6 and 1.7 for fault gas detection results for details, seeing Fig. 1.2.

From the malianying fault gas detection results, it can be seen that H_2 and CO_2 reflect the $F_{2\text{-Qh}}$ of the main front section accurately, and the anomaly of Hg corresponding to $F_{2\text{-Qh}}$ of the main front section is a little south, but Hg reflects the $F_{1\text{-Qp3}}$ of the main rear section accurately, with the highest value of 120 ppm, while H_2 and CO_2 reflect the $F_{1\text{-Qp3}}$ of the main rear section, H_2 is backward and CO_2 is forward. Based on the detection results of Hg, H_2 and CO_2 fault gases on the main front section $F2_{\text{-Qh}}$ and the main rear section $F1_{\text{-Qp3}}$ of Tianzhuang fault, this is basically consistent with the distance between the two sections formed by the fault depression activity of Tianzhuang fault since the early Late Pleistocene revealed by shallow seismic exploration, both of which are 400 m left and right. The $F_{1\text{-Qp3}}$ activity time of the main section at the rear edge is old, but the formed fracture zone is large, and the fault gas is easier to escape. While the $F_{2\text{-Qh}}$ activity time of the main section at the front edge is new, the formed fracture zone is relatively small, and the hanging

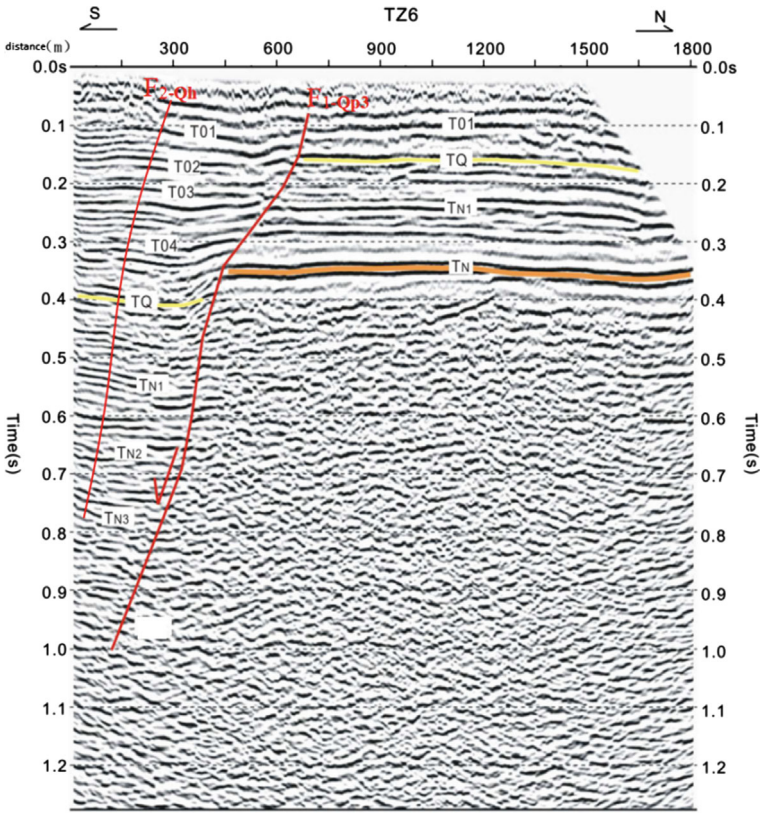

Fig. 1.4 Reflection seismic time profile of mlyl (Malianying Road) survey line of Tianzhuang fault

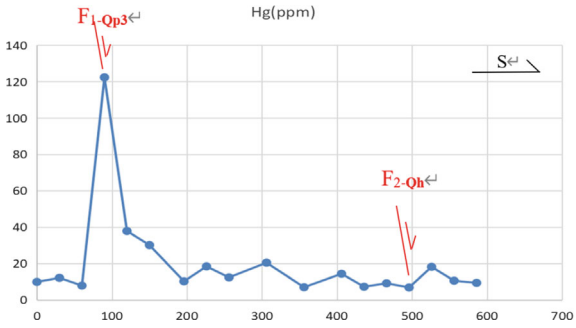

Fig. 1.5 Fault gas Hg survey line of Tianzhuang fault MLYL (Malianying Road)

wall is still in the state of upward compression, so the fault gas is not easy to escape, resulting in small abnormal amplitude.

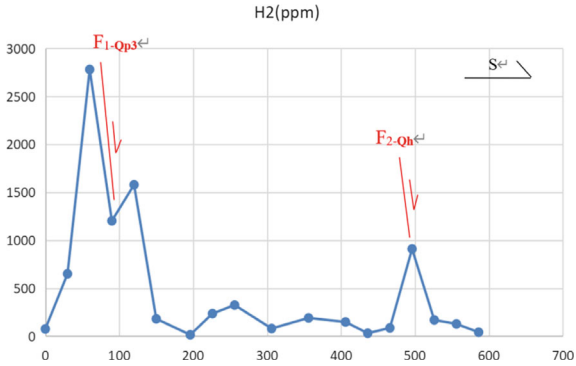

Fig. 1.6 H_2 measuring line of mlyl (Malianying Road) fault gas in Tianzhuang fault

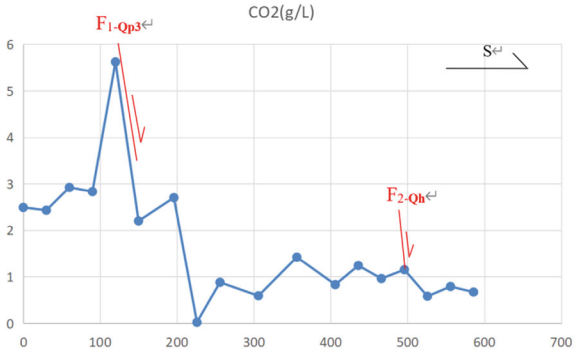

Fig. 1.7 Fault gas CO_2 survey line of Tianzhuang fault mlyl (malianying Road)

1.3.3 Disclosure of $F_{1\text{-}Qp3}$ Details of Main Section by Combined Borehole Profile

According to the strata revealed by this cross-section borehole exploration (see Fig. 1.8), layer ⑤ is the bottom of the Holocene, which is a set of basically continuous brown-yellow fine sand, locally brownish red silty sand or dark brown silty soil. All boreholes are exposed, and the depth fluctuates slightly up and down. It is fluvial facies deposition. Considering that the sampling rate of sand layers in each borehole is inconsistent, it is considered that the Tianzhuang fault has not broken the Holocene stratum.

Layer ⑥ is dominated by Brown silty clay and silt as a whole and mixed with brown-yellow silty sand locally. Rust-yellow fine lines and gray spots can be seen. It is a swamp facies deposit. The basis for the dislocation of this set of strata is first based on the shallow seismic exploration interpretation section, which shows that the reflected wave in-phase axis is obviously misplaced at the depth of 30 ~ 40 m, and the joint drilling section shows that there is a slight dislocation in the stratum at the bottom of layer ⑥, The dislocation of $F_{1\text{-}Qp3}$ of the main section is about 0.4 m.

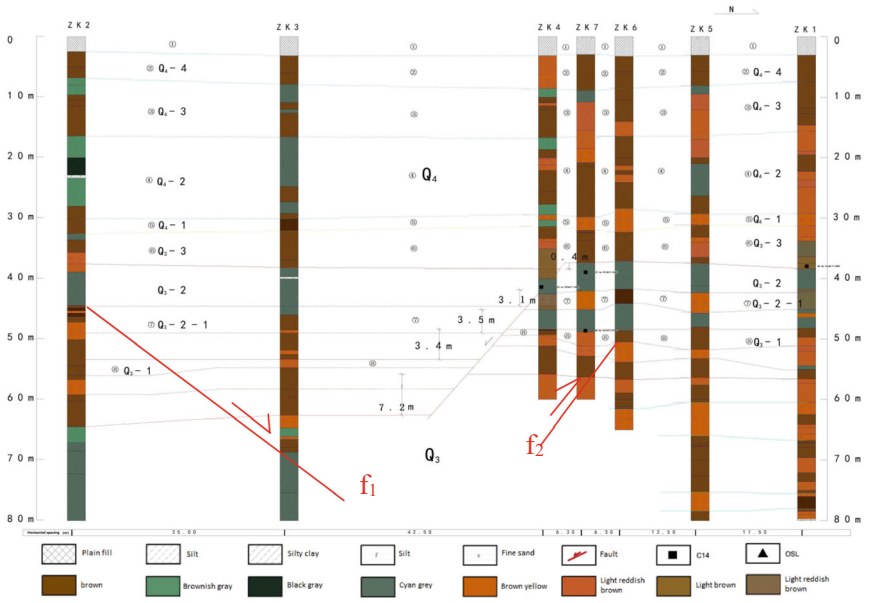

Fig. 1.8 Borehole joint section

Layer ⑦ shows three distinct sets of strata. The upper strata are staggered by the main section $F1_{-Qp3}$ for 3.1 m, and the middle and lower strata are staggered by the main section $F1_{-Qp3}$ for about 3.5 m: the upper strata of layer ⑦ are cyan, grayish cyan, black cyan and grayish brown muddy marker layers, which are mainly fluvial facies deposits. This set of strata can be tracked and identified in the upper and lower walls from lithology, particle size Color and sedimentary facies are compared. The upper part of the stratum corresponding to borehole ZK4 is brown silt and the lower part is cyan-gray silt, which shows obvious differences from the adjacent strata of the upper and lower walls, indicating the change of fault activity on the normal sedimentary environment of the stratum in this section; The middle of layer ⑦ is a continuous and traceable silty sand layer, mainly light reddish brown and brownish yellow silty sand, and brownish yellow silty soil can be seen locally. This set of strata can also be used as a marker layer, mainly fluvial facies deposition; The hanging wall of the lower part of layer ⑦ is dominated by Brown silty clay and silt, and brown-yellow silty sand can be seen locally, with embroidered yellow and calcareous nodules visible. The footwall is dominated by cyan-gray silty clay, with embroidered yellow and calcareous nodules visible locally. The strata of the upper and lower walls of the lower fault of layer ⑦ show obvious differences in sedimentary environment, and the hanging wall is fluvial facies or swamp facies, It shows that the hanging wall can not always be in the underwater environment, and the water level should be shallow. The footwall is swamp facies, the water level is deep and basically maintains the

underwater sedimentary environment. The two sedimentary environments provide good evidence of fault dislocation.

Layer ⑧ can also be divided into three sets of strata: the upper stratum is mainly brown and brown-yellow silt and silty clay, mainly swamp facies deposits; The middle part is dominated by continuous and traceable brown-yellow silt and silt. This layer can also be used as a marker layer, which is fluvial facies deposition; The lower stratum is brown silty clay, and the $F_{1\text{-}Qp3}$ staggered stratum of the main section is 7.2 m, mainly swamp facies.

According to the fault characteristics revealed by the combined borehole profile, it is considered that the target fault is not faulted at the middle and upper part of $Q_{p3\text{-}3}$ (layer ⑥), and the main section $F1_{\text{-}Qp3}$ fault $Q_{p3\text{-}2}$ (layer ⑦), $Q_{p3\text{-}2\text{–}1}$ (middle of layer ⑦) and $Q_{p3\text{-}1}$ stratum can be identified (see Table 4).

Based on the stratigraphic characteristics of the combined borehole profile, it is concluded that the sedimentary thickness of the faulted strata in the descending wall is greater than that of the same layer in the ascending wall, which is consistent with the sedimentary characteristics of the normal fault faulted wall; The staggered distance is about 3 m twice within the exposed depth of the borehole. The coseismic displacement can judge that two main dislocation events occurred in the identification layer, which provides reliable geological evidence for analyzing the seismic risk of Tianzhuang fault; The main section $F1_{\text{-}Qp3}$ of Tianzhuang fault is not faulted with Holocene strata in this site. The faulted strata are three sets of late Pleistocene strata. From top to bottom, the offset of faulted strata gradually increases, which is 0.4, 3.5 and 7.2 m in turn.

There are two associated faults f_1 and f_2 on both sides of the main section $F1_{\text{-}Qp3}$. f_1 is the reverse associated normal fault of the main section $F1_{\text{-}Qp3}$. It can be seen from ZK2 and ZK3 that the stratum has staggered, while f_2 is the co-directional associated reverse fault of the main section $F1_{\text{-}Qp3}$. It can be seen from ZK4, zk7 and ZK6 that the stratum has obviously staggered. From the section, the horizontal distance from ZK2 to ZK6 is 90 m, so it can be seen that the influence range of the deformation zone on both sides of the main section $F1_{\text{-}Qp3}$ of the late Pleistocene can reach 90 m, of which the influence range of the hanging wall deformation zone is about 55 m, the influence range of the footwall deformation zone is about 35 m, and the range of the hanging wall deformation zone of the normal fault is larger than that of the footwall deformation zone. At the same time, the $F_{2\text{-}Qh}$ activity of the main section of Tianzhuang fault is new, but the fracture zone is weaker than the $F_{1\text{-}Qp3}$ of the main section. Therefore, it can be judged that the activity became weaker in the Holocene. The total deformation zone of $F_{2\text{-}Qh}$ of the main section dominated by creep will not be greater than 90 m, and the unilateral deformation zone will not be greater than 55 m.

1.4 Analysis on the Formation Mechanism of the Tianzhuang Fault Deformation Zone

The Tianzhuang fault is part of the Northeast Branch of the Jiaocheng fault and shares its origin with the Jiaocheng fault. During the Mesozoic Yanshan movement, the Qinshui Basin thrust northwestward. In the northwest corner of the Qinshui Basin, where the Taiyuan Basin is located, the western boundary (predecessor of the Jiaocheng fault) thrust toward the Luliang Uplift, while the northern boundary (predecessor of the Tianzhuang fault branch) thrust toward the Wutai complex anticline. As the Cenozoic Himalayan movement commenced, the compression along the southeast-northwest direction transitioned into tension. Throughout the three episodes of Himalayan activity, the thrust faults along the western and northern boundaries of the Taiyuan Basin reactivated in the form of normal fault strike-slip. The Middle and Late Neogene period marked the initial episode, with subsequent early and intermediate episodes dominated by compressive strike-slip uplift. This geological activity is reflected in the Tianzhuang fault's seismic survey line (jb-xbg, Wenjiabao-xiao beige), which reveals a stepped fault depression. The deepest fault depression corresponds to the second phase of the Xishan movement, the sub-deeper fault depression aligns with the fault depression in the initial phase of the third Xishan movement. This is followed by relative compression uplift during the Middle Pleistocene, while the shallowest fault depression corresponds to activity since the late Pleistocene. Overall, the shallowest fault depression activity is attributed to the third phase of the Xishan movement.

In accordance with the characteristics of the Himalayan movement, it comprises alternating phases of compression uplift and tension-induced fault depression. Compression causes a relative retreat of sections in comparison to their initial compressed state, whereas tension propels sections forward relative to their initial tensioned state. Consequently, as a result of the combined effects of preceding overall compression uplift and subsequent continuous tension-induced fault depression, sections migrate, giving rise to a rolling anticline between section groups during the tension phase. This phenomenon serves as a geological basis for delineating the scope of the entire fault deformation zone during this period. However, when considered in conjunction with the specifics of the borehole joint section, it is possible to constrain the substantial influence of deformation to the primary section. This constraint holds significant engineering implications, particularly for the construction of deep structures.

1.5 Conclusion

In summary, the Xishan Sanmu movement has induced multiple instances of fault subsidence within the Tianzhuang fault, with the most recent and shallowest subsidence activity having a significant impact on surface and underground infrastructure.

Through a comprehensive examination of the fault zone, we have observed ground fractures and tension fractures in buildings. Moreover, detailed insights into the deformation zone have been unveiled through drilling joint sections. Consequently, it has been determined that the forward edge's main section (F2-Qh) extends 55 m to the south, while the rear edge's main section (F1-Qp3) extends 35 m to the north. The distance between these two primary sections has been calculated as 400 m, resulting in a total deformation zone width of 490 m. To address the specific seismic fortification requirements of the project, it is advisable to establish a safety margin of 55 m on either side of the two main sections.

Acknowledgements Supported by the national field scientific observation and research station of continental rift dynamics in Taiyuan, Shanxi Province (Project No.norsty20-06); The general nature fund project of Shanxi Provincial Department of science and Technology (No.: 201901d111462).

References

Ge X, Minpei W, Liu J (2010) Redefining the era and background of the Sichuan movement and the initial uplift of the Qinghai Tibet Plateau: enlightenment from the formation of Huangling anticline. Geosc Front 17(4):206–217

Han X, Li B, Dong B et al (2017) Study on the activity of the middle section of Tianzhuang fault. Adv Geophys 33(5):1789–1795

Huang F, Rooney TO, Xu J, Zeng Y (2021) Magmatic record of continuous neo-tethyan subduction after initial India-Asia collision in the central part of southern Tibet. GSA Bull 133(7–8):1600–1612

Lei H, Xinhuai Z, Chiyang L et al (2012) Important turning period of cenozoic basin evolution in bohai Sea–evidence and regional dynamics analysis. Chin Sci Geosci 42(6):893–904

Pan G (1957) Large structure of Datong coalfield, Shanxi. Sci Bull 2(20):633

Wang C, Wu J, Yang T (2018) Double difference tomography in Taiyuan Basin and its surrounding areas. J Geophys 61(3):963–974

Wang Y, Sun L, Zhou L et al (2018) Discussion on the relationship between the Yanshan movement and the destruction of the North China Craton. Chin Sci Geosci 48(5):521–535

Xie X, Xiao Z, Wang W (1996) Study on Mesozoic Cenozoic tectonic evolution of Jinzhong South fault basin and current tectonic stress field in Linfen Basin. Beijing: Institute of crustal stress, China Seismological Bureau

Xu L (2013) Characteristics of active fault system in the central part of North China block and preliminary study on post earthquake risk. Qingdao: China Ocean University

Yang C, Wang W (1999) Yanlie fault zone and Yanqiao structure of Cenozoic rift system in central and southern Shanxi–reanalysis of Cenozoic rift system structure in central and southern Shanxi according to geophysical data. Beijing: Institute of crustal stress, China Seismological Bureau

Zhang L, Dong B, Shi S, et al (2020) Segmentation of activity and seismic risk analysis of the Tianzhuang Fault in the Taiyuan Basin. Geodesy Geodyn 40 (2):204–213

Zhang M, Yang C (1996) On truncated faults and earthquakes-taking three NE trending faults in North China as an example. Chin Earthq 12(2):163–172

Zhu R, Xu Y (2019) Western Pacific plate subduction and North China Craton destruction. Chin Sci Geosci 49(0):1346–1356

Chapter 2
Research Progress and Trend Analysis of Deep Fracture of Deep-Cut Canyon Rock Slope

Bo Wang, Qihua Zhao, and Shenqin Peng

Abstract With the continuous exploration of clean energy by mankind, a large number of hydropower stations have been built in western China. Most of these hydropower stations are located in the gorge surrounding the Qinghai-Tibet Plateau. The gorge are steep and deep, often accompanied by high ground stress. After a series of geological structure movements, such canyons often expose the phenomenon of deep fracture. Such phenomena can reduce the intensity of the peripheral rock body and affect the stability of high-steep slope. Therefore, this article first summarizes the development and distribution characteristics of deep-seated fracture in the slopes of typical hydropower stations. Then, it sorts out the research results of domestic and foreign scholars from the aspects of geomechanics model and genetic mechanism. Finally, on the basis of summarizing the research on deep-seated fracture, the problems and difficulties in the current research are analyzed, and the focus of future research is prospected.

Keywords Deep-cut canyon · Deep-seated fracture · Research summary · Research outlook

2.1 Introduction

Deep fracture is a series of deep relaxation phenomena that develops in deep canyon unloading bands (conventional unloading zone, strong unloading zone, weak unloading zone) and within the micro-new rock mass, which belongs to a special form of rock mass fracture. Deep fractured rock masses generally exhibit slight

B. Wang · Q. Zhao (✉) · S. Peng
State Key Laboratory of Geo-Hazard Prevention and Geo-Environment Protection, Chengdu University of Technology, Chengdu 610059, Sichuan, People's Republic of China
e-mail: zhqh@163.com

B. Wang
e-mail: wb510911219@163.com

S. Wang et al. (eds.), *Engineering Geology for a Habitable Earth: IAEG XIV Congress 2023 Proceedings, Chengdu, China*, Environmental Science and Engineering,
https://doi.org/10.1007/978-981-99-9065-8_2

weathering, partially affected by groundwater, and the degree of weathering is relatively strong (Li 2015). This kind of phenomenon becomes a place for groundwater movement and storage, which has a certain impact on the quality and strength of the rock mass, or as a structural plane that affects the stability of the rock mass, further affects the stability of high and steep slopes, and prolongs the construction period of the dam site of the hydropower station, the related treatment measures and the impact of project construction have become one of the restrictive factors restricting large-scale project construction activities (Han 2015; Chen 2014).

During the survey of some large hydropower stations in southwestern China in the 1980s, a large number of deep fractures were revealed. At that time, the concept of deep fractures had not yet been formed. Han et al. first defined it as "loose rock mass" in the process of studying the location characteristics of Daliushu Hydropower Station, and believed that its driving force was formed by both gravity and seismic and geological forces (Han et al. 1993). In the research of Miaojiaba Hydropower Station, Yang Yongming called the deep fractures as a deformed wedge, and believed that the wedge was caused by a long-term partial deep unloading deformation process, which was then caused by gravity creep (Yang 1995). Since then, many domestic scholars (Yan et al. 2005; Chen et al. 2005a, 2005b; Wang et al. 2008; Qi et al. 2004; Li et al. 2007; Liu 2016; The Rock Mass in the Dam Area of Baihetan Hydropower Station 2011) have had a preliminary understanding and research on the phenomenon of deep fractures. Foreign research on deep fracture phenomenon was later. In the mid-1990s, Stini first discovered this kind of phenomenon and defined it as Deep-seated Gravitational Slope Deformation (DSGSD). Later foreign scholars (Seno and Thüring 2006; Crosta et al. 2006; Hradecký and Pánek 2008; Willerich et al. 2009; Ambrosi and Crosta 2006) also carried out this phenomenon. A large number of studies have their own definitions such as: Deep-seated Large Scale Rock Slides, Sackung, Deep Seated Distortion, Lateral Spreading, Mass Rock Creep, etc. (Han 2015).

The above research laid the prototype of deep fracture research. Different deep canyon areas, different experts have different understanding, and the focus of research also has its own focus on their own focus. With the in -depth research on the deep fracture, many scholars have carried out a lot of research on the causes, mechanisms and geological mechanics models of deep fracture, which has good guiding significance for deep understanding of deep cracks. This article reviews the research trend at home and abroad for the phenomenon of deep fracture and further analyzes.

2.1.1 Distribution Characteristics of Deep Fracture Development

With the continuous development of energy in my country, many large and medium-sized hydropower stations have been built in the southwestern region surrounding the Qinghai-Tibet Plateau, such as: Baihetan Hydropower Station, Jinping I and II